First principle studies on lattice thermal conductivity and thermoelectric properties of $LiYSe_2$.

Elkana Rugut[1], Daniel Joubert[1] and Glenn Jones[2]

[1] The National Institute for Theoretical Physics, School of Physics and Mandelstam Institute for Theoretical Physics, University of the Witwatersrand, Johannesburg, Wits 2050, South Africa.

[2] Johnson Matthey Research (PTY) Limited, Scientia, CSIR Campus, Meiring Naude Road, Brummeria, Pretoria, South Africa.

E-mail: elkanatawich@gmail.com

Abstract. Thermoelectric materials can convert heat into electricity, hence these materials can play an important role in the efficient use of energy. In this study, we investigate the structural, dynamical and mechanical stability of lithium yttrium selenide ($LiYSe_2$) alongside its lattice thermal conductivity, electronic transport and thermoelectric properties for the first time. The potential of a material to be used as the active component in the design of a thermoelectric device is based on the value of its figure of merit (ZT), which requires information on the lattice and electronic transport properties. We computed the ZT value within density functional theory using linearized Boltzmann transport equations in a relaxation time approximation. From our findings, $LiYSe_2$ is stable and exhibit a semiconducting character having an indirect band gap of 1.80 eV. The predicted values of the anisotropic lattice thermal conductivity at 300 K are 2.63, 2.58 and 1.09 W/mK for x-,y- and z-axis, respectively, which is favorable for thermoelectric applications. Highest value of the predicted ZT is 0.6 at high temperature of 1000 K when the hole concentration is 10^{19} cm^{-3}, which indicates that with further tuning, $LiYSe_2$ holds potential in high temperature thermoelectric applications.

1. Introduction

Thermoelectricity is perceived as one of the possible solutions to deal with the global energy crisis [1]. The grand challenge in this field is that near room temperature; alloys of bismuth telluride [2] which are dominantly used in fabricating thermoelectric devices for commercial applications have dimensionless figure of merit (ZT) of about unity, which translates to a relatively low efficiency in thermal to electrical energy conversion without any mechanical component. Hence, comprehensive studies [1] have been vigorously explored in the recent years to uncover new potentially viable materials, or to engineer the existing ones in such a way that their ZT is improved beyond unity for efficient large scale production as well as applications.

Regarding the ternary compound of interest; Ohtani *et. al* [3] carried out synthesis of $LiYSe_2$ among other ternary chalcogenides whereby they reported that $LiYSe_2$ can adopt two different types of structures, a NaCl type and α-$NaFeO_2$, depending on the ratio of lanthanide ion (Y) to alkali metal (Li) radius ratio whereby for large (small) radius ratio values, the compound crystallizes in a disordered NaCl structure (α-$NaFeO_2$). Besides the cation radius ratio, the two crystals types are also dictated by the quenching temperatures whereby the NaCl structure is attained when quenched from the higher temperatures whereas α-$NaFeO_2$ structure is obtained when cooled slowly at room temperature [3]. The figure of merit is a quantitative parameter

that describes how efficient a thermoelectric material is in the direct conversion of temperature differences (thermal energy) to electric voltage and vice versa [4]. It is a dimensionless quantity that is related to the Carnot efficiency of a system (η) and is expressed as [5, 6];

$$ZT = \frac{S^2\sigma T}{\kappa} = \frac{S^2\sigma T}{\kappa_e + \kappa_l}; \qquad \eta = \frac{T_h - T_c}{T_h}\frac{\sqrt{1+ZT}-1}{\sqrt{1+ZT}+1} \tag{1}$$

The Seebeck coefficient, electrical conductivity, temperature in Kelvin scale and the total thermal conductivity are denoted by S, σ, T and κ, respectively. The total lattice thermal conductivity has two components, namely the electronic contribution (κ_e) and the lattice contribution (κ_l). For the Carnot efficiency, T_h and T_c denotes the temperature of the hot and cold part of the thermoelectric generator, respectively. Hence for us to gauge how efficient $LiYSe_2$ is; we computed its figure of merit based on first principles within Density Functional Theory (DFT).

2. Methodology

We describe the structural, vibrational, energetic, mechanical, electronic, thermal, transport and thermoelectric properties of lithium yttrium selenide based on numerical simulations conducted using the Vienna *ab initio* simulation package (VASP) [7] that applies the formalism of density functional theory. In order to test the reliability of our results, structural, energetic and mechanical studies were carried out using three functionals namely: local density approximation (LDA) [8], generalized gradient approximation with the Perdew-Burke-Ernzerhof (PBE) [9], as well as PBEsol [10]. The energy cut-off for the plane wave expansion was fixed at 520 eV. The atomic forces and energies were converged within 10^{-4} eV/Å and 10^{-8} eV, respectively, for structural calculations. For elastic constant calculations, the stress-strain technique proposed by Shang *et al.* was applied [11].

Vibrational studies were performed using the Phonopy code [12] where a finite displacement technique was applied on a 3×3×3 supercell with a Monkorst-Pack grid of size 3×3×3 used to sample the Brillouin zone in order to obtain the second and third order inter-atomic force constants from Phonopy and Phono3py [13], respectively. A mesh size of 38×38×24 was found sufficient to obtain converged values of lattice thermal conductivity. We computed the electronic transport coefficients by solving Boltzmann transport equations based on DFT under the mode dependent relaxation time approximation as implemented in BoltzTraP2 [14]. Both lattice thermal conductivity results and transport coefficients were then incorporated onto equation (1) as also indicated in the step by step work flow provided in Figure 1 (center) in order to predict the dimensionless figure of merit of $LiYSe_2$.

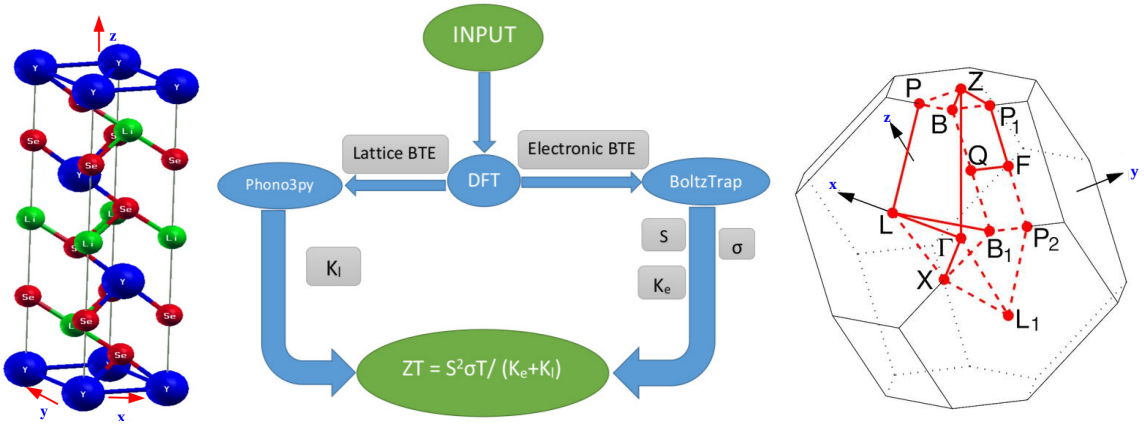

Figure 1. Crystal stucture of $LiYSe_2$ (left), work flow (center) and its Brillouin zone [15] (right)

3. Results and discussion

Structural, energetic and mechanical studies of $YCuSe_2$ were conducted using three functionals, as shown in Table 1. By comparing the obtained values of structural properties with the existing experimental data; we deduced that among the three functionals considered, PBEsol describes the structural behavior of $LiYSe_2$ better relative to PBE and LDA. Hence, further in-depth studies of lattice thermal conductivity and transport properties were investigated using PBEsol. The negative values obtained for cohesive energies signify that $LiYSe_2$ is an energetically stable.

Table 1. Structural parameters and cohesive energy.

	a (Å)	c (Å)	V_o (Å^3)	α (°)	γ (°)	B (GPa)	E_{coh} (eV/atom)
PBE	4.078	19.583	282.036	90	120	40.76	-2.471
LDA	3.985	19.135	263.157	90	120	48.95	-5.125
PBEsol	4.031	19.357	272.392	90	120	44.43	-4.801
Exp [3]	4.048	19.440	275.870	90	120	-	-

3.1. Mechanical properties

The elastic coefficients, bulk modulus, shear modulus and Young's modulus provided in Table 2 are in gigapascals (Gpa). Basically, $LiYSe_2$ belongs to the trigonal crystal system as shown in Figure 1 (left) of point group $\bar{3}$, Hermann Mauguin R$\bar{3}$m and space group number 166 falling under Rhombohedral (I) class as per classification of Coudert and Mouhat [16].

Table 2. Mechanical properties.

Functional	C_{11}	C_{12}	C_{13}	C_{14}	C_{33}	C_{44}	B	G	E	ν	G/B
PBE	101.15	27.82	23.19	-0.22	77.87	26.70	46.55	31.51	76.57	0.23	0.68
PBEsol	97.57	26.07	21.03	0.03	72.92	25.94	44.40	30.47	74.39	0.22	0.69
LDA	95.88	25.55	19.07	-1.64	71.29	23.28	42.81	29.02	71.01	0.22	0.68

Therefore, six independent elastic coefficients were obtained as indicated in Table 2. Thus, in order to attain mechanical stability; it has to fulfill the following necessary and sufficient conditions [16].

$$C_{11} > |C_{12}|; C_{44} > 0; C_{13}^2 < \frac{1}{2}C_{33}(C_{11} + C_{12}); C_{14}^2 < \frac{1}{2}C_{44}(C_{11} - C_{12}) = C_{44}C_{66} \quad (2)$$

Since all the four conditions were satisfied, our calculations confirm that lithium yttrium selenide is mechanically stable. Thermoelectric devices should possess exceptional mechanical properties as they might be used in environments where temperature keeps fluctuating. Moreover, their Fratserich's ratio (G/B) [17] is greater than 0.571 for all the three functionals, indicating that $LiYSe_2$ is a brittle material. From the values of Poisson's ratio obtained (≈ 0.22), it indicates the bonding in $LiYSe_2$ is most likely ionic in nature [18].

3.2. Dynamical and electronic properties

From the phonon dispersion curves shown in Figure 2, there is an absence of imaginary frequencies indicating $LiYSe_2$ is thermodynamically stable [12]. From the partial density of states (PDOS), vibration of selenium atoms dominates the acoustic phonons whereas lithium atoms are major heat carriers in the optical region as they propagate actively at higher frequencies. On the other hand, yttrium contributes to both acoustic and optical modes.

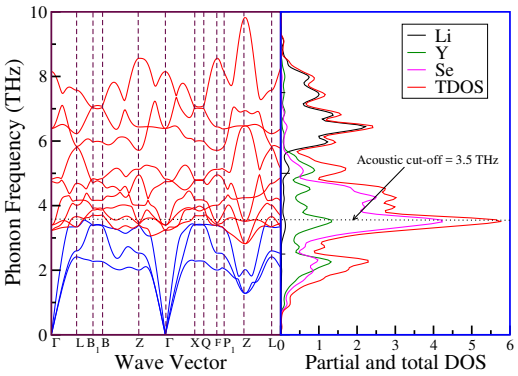

Figure 2. Phonon dispersion.

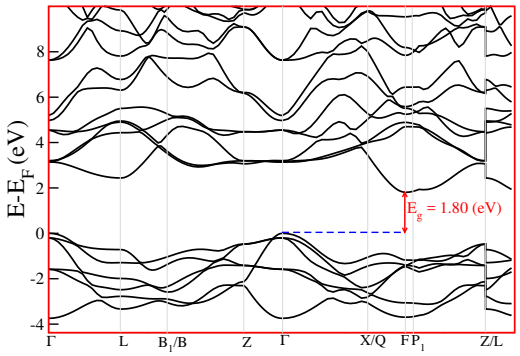

Figure 3. Electronic bands.

The modified Becke-Johnson potential (mBJ) [19] was used in determining the electronic band structure of $LiYSe_2$ in order to open the fundamental gap that is often underestimated when computed using DFT-GGA's. $LiYSe_2$ exhibited a semiconducting character having an indirect band gap of 1.80 eV; whose valence band maxima is situated at Γ whereas the conduction band minima is at F-point in the Brillouin zone as shown in Figure 3.

3.3. Lattice thermal conductivity

Figure 4 shows the lattice thermal conductivity of $LiYSe_2$ which confirms that there is slight thermal anisotropy in that the lattice thermal conductivity is comparable in x- and y-axis (in-plane) but different in the z-axis (out-of-plane).

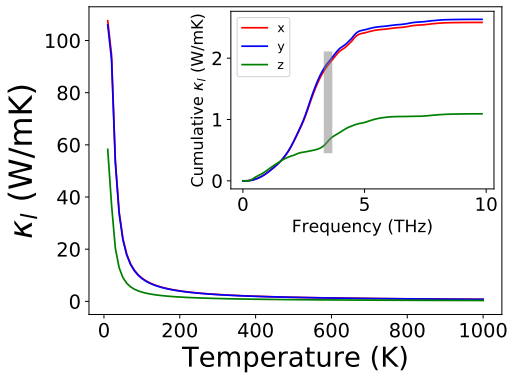

Figure 4. Lattice thermal conductivity and its cumulative.

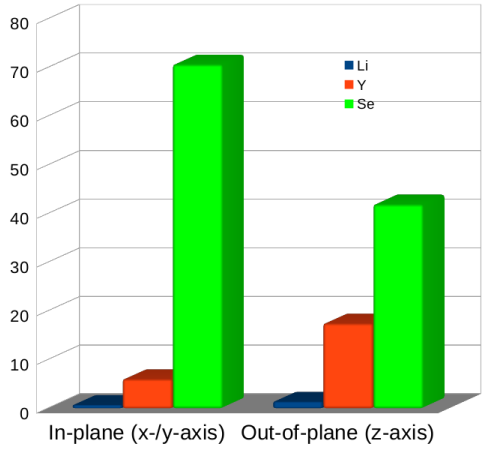

Figure 5. Estimates of percentage elemental contributions.

Similar anisotropic behavior is also visible in the cumulative lattice thermal conductivity as shown in the inset plot. The acoustic cut-off frequency (≈3.5 THz), indicated with the shadowed grey region in the inset plot that highlights the upper bound of acoustic phonon branches in Figure 2, the cumulative lattice thermal conductivity is almost flat at higher frequencies, which signify that acoustic phonon branches dominates heat transport in $LiYSe_2$ compared to the optical phonons. The predicted values of lattice thermal conductivity are 2.63, 2.58 and 1.09 W/mK for x-,y- and z-axis, respectively, at 300 K which is favorable for thermoelectric applications.

In Figure 5; after realizing that acoustic phonons are dominant heat carriers, we further narrow down to examine and approximately quantify the elemental contributions to the total cumulative lattice thermal at the acoustic phonon region at a temperature of 300 K. It is clear that among the three elements; selenium (Se) contributes significantly, followed by yttrium (Y) whereas contribution from lithium (Li) is almost insignificant. In addition; for the case of selenium, it indicates that a lot of heat is generated when selenium atoms are propagating in the x-/y-axis ($\approx$ 70%) as compared to the case when they are propagating along the z-axis ($\approx$ 40%). This information is crucial in thermal engineering of $LiYSe_2$ when tuning its lattice thermal conductivity as it indicates which element vibrates a lot relative to other elemental components in this ternary compound.

3.4. Transport and thermoelectric properties

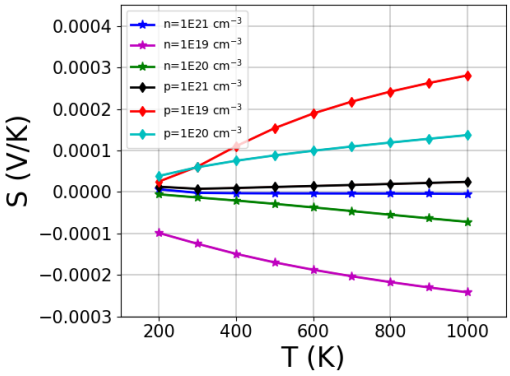

Figure 6. Seebeck coefficient (S) vs. temperature.

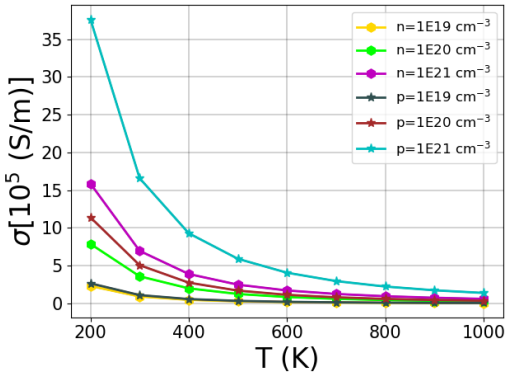

Figure 7. Electrical conductivity (σ) vs. temperature.

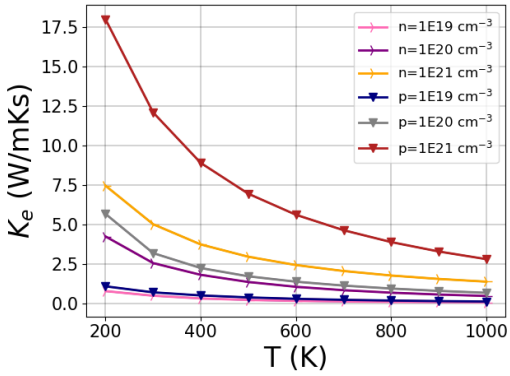

Figure 8. Electronic contribution to thermal conductivity (κ_e) vs. temperature.

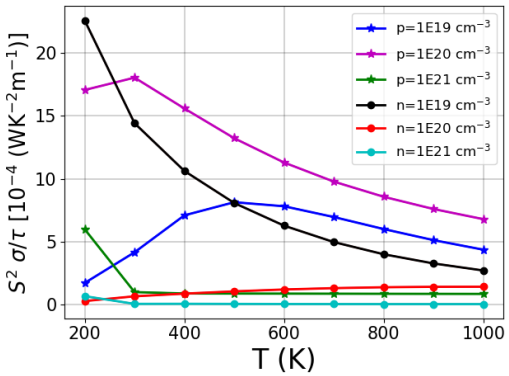

Figure 9. Power factor ($S^2\sigma$) vs. temperature.

Figures 6 to 11 shows the Seebeck coefficient (S), electrical conductivity (σ), electronic contribution to thermal conductivity (κ_e), power factor ($S^2\sigma$) and figure of merit (ZT) as function of tempereture, for various electron and hole concentrations. The highest value of Seebeck coefficient is attained when hole concentration is 10^{19} cm^{-3}, as displayed in Figure 6. Highest value of electrical conductivity is obtained when hole concentration is 10^{21} cm^{-3}

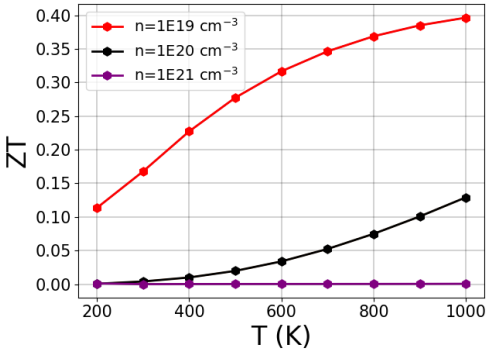

Figure 10. ZT for electrons.

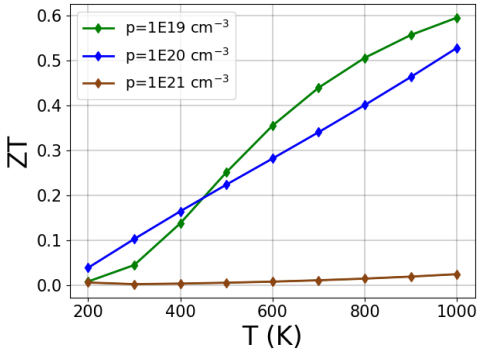

Figure 11. ZT for holes.

as presented in Figure 7. Lowest value of κ_e is attained when charge carrier concentration is 10^{19} cm^{-3} as shown in Figure 8. Above 300 K; highest power factor is obtained when hole concentration is 10^{20} cm^{-3} as provided in Figure 9. Generally, the magnitude of figure of merit is larger for holes relative to electrons as can be seen in Figures 10 and 11. Highest ZT of 0.6 obtained when hole concentration is 10^{19} cm^{-3} could be attributed to its high Seebeck coefficient and low values of electronic contribution to thermal conductivity (κ_e).

4. Summary and conclusion

We have performed a comprehensive study on structural, vibrational, energetic, mechanical, electronic, thermal, transport and thermoelectric properties of $LiYSe_2$ based on the first principles. We confirm that it is a stable ternary compound. From the value of ZT obtained (0.6); with further tailoring, $LiYSe_2$ holds promising potential in thermoelectric applications in that via thermal engineering i.e through creation of selenium (Se) vacancy defects; its ZT can be tuned towards unity.

Acknowledgments

We are grateful to Johnson Matthey Technology Centre (Pretoria) for financial support and Centre for High Computing (Cape Town) for computational resources.

References

[1] T. Tritt, Annual review of materials research. **41**, (2011) 433-448.
[2] L. Hu, T. Zhu, Y. Wang, H. Xie, Z. Xu, X. Zhao, NPG Asia Materials. **6**, (2014) e88.
[3] T. Ohtani, H. Honjo and H. Wada, Materials research bulletin. **22**, (1987) 829-840.
[4] J.P. Heremans *et al.*, Science **321**, (2008) 554-557.
[5] M. M. Rull-Bravo, J. F. Fernandez and M. Martin-Gonzalez, Rsc Advances. **5**, (2015) 41653-41667.
[6] B. Sherman, R. R. Heikes and R. W. Ure , Journal of Applied Physics. **31**, (1960) 1-16.
[7] G. Kresse, J. Hafner, Physical Review B. **47**, (1993) 558.
[8] A. D. Becke, Physical review A. **38**, (1988) 3098.
[9] J. P. Perdew, K. Burke and M. Matthias, Physical review letters. **77**, (1996) 3865.
[10] M. Ropo, K. Kokko, and L. Vitos, Physical Review B. **77**, 195445.
[11] Shang S, Wang Y and Zi-Kui L 2007 *Appl. Phys. Lett* **90** 101909.
[12] A. Togo and I. Tanaka, Scripta Materialia. **108** (2015) 1-5.
[13] A. Togo, L. Chaput and I. Tanaka, Physical Review B. **91**, (2015) 094306.
[14] M. K. Georg, C. Jesús and M. J. Verstraete, Computer Physics Communications. **231**, (2018) 140-145.
[15] S. Curtarolo *et. al*, Computational Materials Science.**58**, (2012) 218-226.
[16] F. Mouhat and F. Coudert, Physical Review B. **90**, (2014) 224104.
[17] Tariq S, Ahmed A, Saad S and Tariq S 2015 *AIP Adv.* **5** 077111.
[18] J. Haines, J. M. Leger and G. Bocquillon, Annual Review of Materials Research. **31**, (2001) 1-23.
[19] F. Tran and P. Blaha, Physical review letters. **102**, (2009) 226401.